AIMS Materials Science, 10(4): 575–588.
DOI: 10.3934/matersci.2023032
Received: 16 April 2023
Revised: 22 June 2023
Accepted: 04 July 2023
Published: 21 July 2023

http://www.aimspress.com/journal/Materials

Research article

Energy consumption and surface roughness maps for low and moderate speed machining of Aluminum alloy 2014: An experimental study

Umer Shaukat[1,*], Scott Gohery[2,*] and Tesfaye Molla[2,*]

[1] Department of Mechanical Engineering, Pakistan Institute of Engineering and Applied Sciences, Nilore, Islamabad, Pakistan
[2] Department of Mechanical Engineering, the University of Melbourne, Parkville, VIC 3010, Australia

* **Correspondence:** Email: umershaukat67@gmail.com, scott.gohery@unimelb.edu.au, scott.gohery@gmail.com, tesfaye.molla@unimelb.edu.au.

Abstract: The rising energy prices and soaring environmental concerns have put an immense pressure on the wide usage of machining processes. The total power consumption during machining includes the power consumed by the machine itself and the power used to remove the material from the workpiece. An accurate prediction of energy consumption during the machining process is the basis for energy reduction. In this study, the specific cutting energy and surface finish for low and moderate-speed orthogonal machining of the aluminum alloy 2014 are evaluated. The measured values for the specific cutting energy and surface roughness are presented as maps on a grid, which is based on the machining parameters including the following: (1) cutting speed and (2) undeformed chip thickness. The specific cutting energy map depicts low energy consumption values of 0.52 J/mm^3 for the aluminum alloy 2014 at medium speed machining. The roughness maps depict high roughness values at high cutting speeds. Both maps help in optimizing the machining process to achieve a required surface roughness with minimal energy consumption. A review of a specific cutting energy map demonstrates that energy consumption decreases by increasing the cutting speeds. The decrease in energy consumption at moderate speeds corresponds to the low cutting forces. This potentially happens as a result of thermal softening of the material caused by adiabatic heating. This subsequently leads to an increase in the machinability of the aluminum alloy 2014 at moderate cutting speeds. Furthermore, the decreasing chip thickness and increasing shear angle as a result of

increasing the cutting speed confirms the increased machinability of the workpiece at moderate speeds.

Keywords: energy map; specific cutting energy; roughness map; cutting forces; chip thickness; experimental study

Abbreviations: *MRR*: Material Removal Rate (mm^3/s); *SCE*: Specific Cutting Energy (J/mm^3); F_c: Cutting Forces (N); P_{air}: Power Consumption without any Contact (W); P_{cut}: Power Consumption for the Actual Cut (W); *d*: Depth of Cut (mm); *f*: Feed Rate (mm/rev); *r*: Chip Thickness Ratio; t_c: Actual Chip Thickness after Machining (mm); t_o: Undeformed Chip Thickness (mm); *v*: Cutting Speed (m/min); *w*: Depth of Cut (mm); φ: Shear Angle (Degrees)

1. Introduction

Pure aluminum or aluminum alloys (Al-alloys) with a low percentage of alloying elements are renowned for their low hardness and low wear resistance characteristics. The augmentation of alloying elements enhances the mechanical properties and surface characteristics of the base metal [1]. The aerospace industry has a great interest in the use of aluminum alloys due to their excellent density combined with their mechanical properties; in particular the 2000 and 7000 series of aluminum alloys account for a large proportion of aircraft components. The application of Al-alloys further extends to the marine and automotive industries, the production of sports equipment and various types of tools and machinery [2]. For example, aluminum alloy 5A06 possesses an enhanced strength and corrosion resistance, as well as an improved welding performance, which are suitable for machining and formability [3]. Furthermore, porous high entropy alloys (HEAs) containing aluminum have shown some promising results in terms of its enhanced hardness, fracture toughness, and corrosion and wear resistance [4].

The products made of aluminum are often required to be produced as a single piece through the machining process [5]. However, the abatement of fossil fuel reserves and increasing concerns of environmental safety and conservation has led to an extensive examination of the machining processes [6]. A literature review reveals that 17% of the ownership of a machine tool accounts for the cost of energy consumption [2]. The urgency of developing machining techniques to lower energy consumption with the development of desired mechanical properties is greater than ever [7–11]. The quality of a machining process is defined by its economics. In addition, the final properties of the machined material also play a significant role in defining the machining process efficiency [12]. Therefore, there is a need for developing new methods and techniques to acquire the desired mechanical characteristics with a low environmental and economic impact [13,14].

Traditional cooling agents, including fluids and/or lubricants, are utilized to maximize the productivity of machining processes. However, the application of such lubricants could negatively affect the economics of the machining process [15–19]. Dry machining leads to higher surface alterations due to higher thermal effects, though it has less of an economic and environmental impact. To control the cutting temperatures and to improve the machinability of materials, conventional cutting fluids, such as air and water, are often used. Recently, cryogenic cooling with liquefied gases has become the focus of many researchers as a technique to control the temperature in the machining

of difficult-to-machine materials. Furthermore, auxiliary systems like pumps, fans, and ACs consume a lot of energy during the machining process [20].

Energy dissipation during machining occurs in two ways: (1) when electricity is not used to cut the material through the insert, and (2) when the actual material is removed. These states are referred to as basic states and cutting states, respectively [21–23]. The energy consumed during the removal of one cubic meter of a material is referred to as the specific cutting energy (SCE) and is measured in the units of J/mm^3 [13]. SCE effectively defines the efficiency of the machining process and is independent of the type and make of the tool used during machining [24].

Draganescu et al. [25] demonstrated that the SCE consumption is low at high-speed machining parameters. For high-speed machining of Inconel, Pawade et al. [26] demonstrated that the SCE is significantly affected by the changes in the feed rate. Balogun and Mativega [27] also explored the effects of the feed rate on the SCE. They demonstrated that a low feed rate increases the values of the SCE, which subsequently affects the plowing effect of the tool. Warsi et al. [28] performed a detailed optimization of the SCE and the material removal rate in the machining of the aluminum alloy 6061-T6 at a high speed. The results showed that, with the proper selection of cutting parameters, the removal of the material can be enhanced by 33%, with a 5% decrease in energy consumption. Previous studies have demonstrated that the surface integrity and chip morphology of workpieces affects the SCE [29,30].

In a machining technique, the SCE is closely related to the cutting parameters such as cutting speed, feed rate, and the geometry of the tool [31]. Among these parameters, feed rate and cutting speed significantly affect the surface finish, the SCE, the production time, the tool life, and the cutting temperatures [32–34]. If the cutting parameters are not optimized, the production time and energy consumption may potentially increase, and the surface finish may become poor. Optimization of the cutting parameters can be achieved by the development of process maps based on the performance of the material, making them easily available and accessible to local machinists. The benefit of process maps for orthogonal machining (OM) operations has been thoroughly discussed in literatures [24,35].

The literature survey reveals that energy consumption during the machining of the aluminum allow 2014 has not been studied to date. As such, this study aims to develop process energy maps (SCE) as a function of critical cutting parameters (i.e., cutting speed and feed rate) for the aluminum alloy 2014. In addition, the study also presents roughness maps for the same material. The study is carried out at low and moderate cutting speeds, taking into account the effects of cutting forces, chip thickness, and shear angle.

2. Materials and methods

In this section, the determination and analysis of the SCE, cutting forces, surface roughness, chip thickness, and shear angle are thoroughly discussed. The experimentation utilized a YIDA ML-300 CNC machine, which possesses a total power of 26 kW. A bar of aluminum alloy 2014 with of length 300 mm and diameter of 160 mm was utilized. In all of the targeted experiments, the length of the cut was kept at a constant value of 75 mm. During the machining operation, a Yokogawa power analyzer CW-240 was employed to measure the power consumption. The measurement of the surface roughness was performed with a TIME 3110 roughness tester. The chip thickness was measured with the help of a Mitutoyo thickness gauge, as shown in Figure 1. For machining of the

workpiece, uncoated cutting inserts (CCMW-09 T3 03-H13A) manufactured by Sandvik Coromant industry [36] were used under a dry condition. They used an OM technique for their study. OM is a two-dimensional machining technique which is usually employed to simplify complex three-dimensional machining operations [37–40].

For the proper application of OM, a cut of a constant depth of 4 mm was selected. The depth of cut is similar to the one considered in Warsi et al. [24]. This enabled us to make a comparison between SCE values of the aluminum alloy 2014 with the SCE values of the aluminum alloy 6061-T6 as calculated by Warsi et al. for similar experimental conditions. The objective is to develop energy and roughness maps for low and medium speed machining. The cutting speed and feed rate were selected accordingly, as given in the design of experiments (DOE) in Table 1. Moreover, the selected values for the feed rate are shown in Table 2.

Figure 1. Mitutoyo ABS digital thickness gauge used for the measurement of chip thickness.

Table 1. Cutting Speed and its levels.

Parameter	Level 1	Level 2	Level 3	Level 4	Level 5
v (m/min)	250	500	750	900	1000

Note: Depth of cut is kept constant at 4 mm.

Table 2. Feed Rate and its levels.

Parameter	Level 1	Level 2	Level 3	Level 4	Level 5	Level 6	Level 7
f (mm/rev)	0.1	0.15	0.2	0.25	0.3	0.35	0.4

Note: Depth of cut kept constant at 4 mm.

During the experiment, a fresh insert was used. The measurement of power was completed in two stages. In the first stage, the tool was moved along the length of the workpiece without any direct contact between the tool and workpiece and power consumption was measured (P_{air}). In the second stage, power consumption was measured for the actual cut (P_{cut}). The difference between the two values gave the actual power consumption during the machining operation (P_{actual}). The specific energy consumption is the ratio of power consumption during the machining operation to the

material removal rate, as given by Eq 1 [41–44]:

$$SCE = \frac{P_{cut} - P_{air}}{v \times f \times d} \tag{1}$$

Roughness was measured from four different locations of the workpiece and an average value was employed for the development of the surface roughness map. The completed schematic used to develop the SCE and the roughness map for the aluminum alloy 2014 is shown in Figure 2. Power consumption can be employed for the calculations of cutting forces [42]. Many researchers have proposed that the SCE can be used to approximate the cutting forces [41–44].

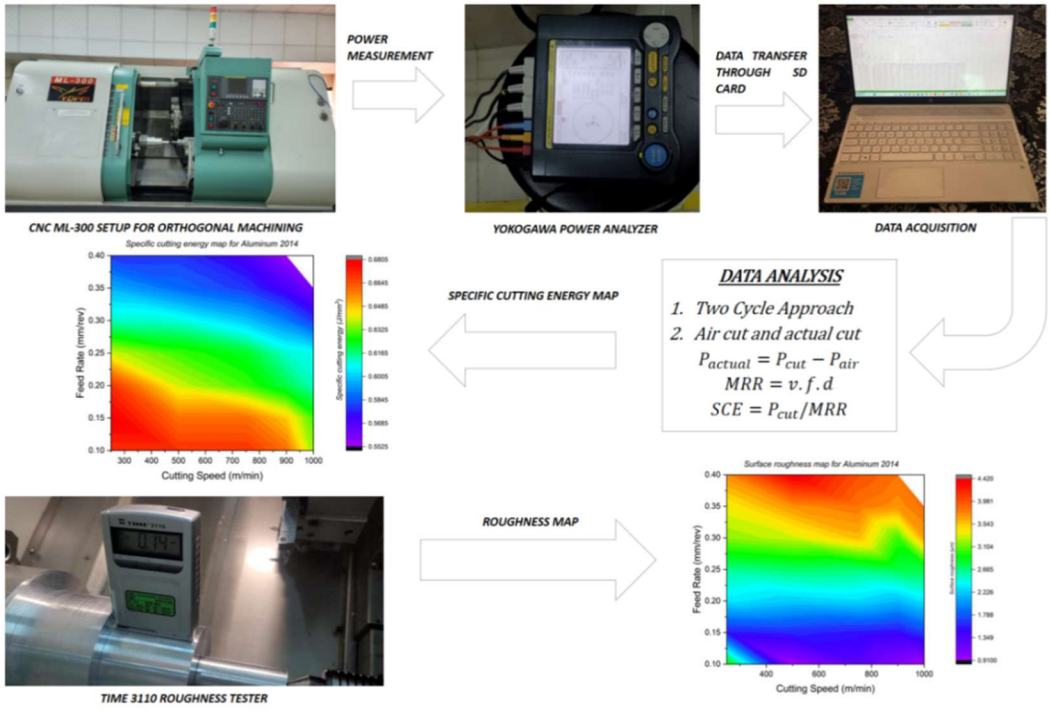

Figure 2. Experimental setup for energy and roughness map development.

In this study, energy consumption was employed to calculate the cutting forces. The specific cutting energy is not affected by the make, type, or efficiency of the tool used to remove the material from the workpiece. It is the ratio of the cutting force (F_c) to the area projected by the cut surface, as given in Eq 2 [41–44]:

$$SCE = \frac{F_c}{w \times t_0} \tag{2}$$

The units' balances and their interpretation associated with *SCE* and F_c are provided in Appendix A.

In this work, the chips obtained by the turning of the aluminum workpiece were measured by the Mitutoyo thickness gauge. The thickness was noted and chip thickness ratio (r) was measured. In

the current study, a rank angle of 0^o was employed. The shear angle (φ) can be calculated using Eq 3 [44]:

$$\tan(\varphi) = \frac{t_0}{t_c} \tag{3}$$

According to Tables 1 and 2, a total of 34 experiments were performed. With the help of a power analyzer and a roughness tester, the SCE and roughness were measured, respectively. The values of the SCE and roughness were plotted on a cutting speed and feed rate grid. The contours for the SCE values were made, which identified the regions of high or low energy consumption and likewise for the roughness map.

3. Results and discussion

The cylindrical workpiece of the aluminum alloy 2014 was subjected to OM and a SCE map was developed under the conditions given in Tables 1 and 2. The energy map is shown in Figure 3. Interestingly, the upper right-hand corner of the map shows the lowest energy consumption values, depicting that at speeds ranging to 1000 m/min with a feed rate of 0.4 mm/rev, energy consumption is reduced significantly. These low values of SCE at a moderate speed depict high production rates with very low energy consumption. In the developed energy map, the left side illustrates the region associated with a high energy consumption.

Contrary to the SCE map, the roughness map is slightly different, as shown in Figure 4. Surface-roughness increases when the feed rates and cutting speeds are high and medium, respectively. However, moderate values of surface finish were demonstrated to be approximately 0.2 mm/rev of an undeformed chip thickness for all the cutting speeds. At this range, the SCE maps reveal moderate values of energy consumption. Therefore, a compromise can be made between the surface finish and energy consumption to obtain the required characteristics with the smallest energy utilization. Both these maps potentially help the machinist to optimize the machining process according to his/her requirement.

Shear angle and chips thickness have been of a great importance in the context of material removal. Shear angle helps us to determine the amount of force required to cut a material. A small shear angle means less force, which can lead to an improved tool life and surface finish. Chip thickness affects the heat generated during the machining operation. A thinner chip will generate less heat, which can help to improve tool life and surface finish. The machinability of a material is usually defined in terms of the shear angle and is a function chips thickness [45]. The plot of chip thickness against cutting speed is provided in Figure 5. Increasing the cutting speed seems to have a detrimental impact on chip thickness. For the calculation of the shear angle, Eq 3 was used. According to Figure 6, an increasing trend of the shear angle is correlated with an increase in cutting speed.

In addition to all of these parameters, a decrease in SCE at a moderate cutting speed can be explained with the help of the cutting forces. As seen in Figure 7, regarding the variation of cutting forces with undeformed chip thickness, at higher feed rates, the cutting forces rise significantly. This occurs because at higher feed rates, the material to be removed in one signal rotation of the workpiece increases. On the contrary, higher speeds lead to a decrease in forces. This boils down to

the fact that the material is subjected to adiabatic heating, which softens at moderate cutting speeds. When this happens, the material removal becomes much easier. Consequently, this reduces the chip thickness and increases the shear angle, thereby increasing the machinability of the workpiece [45].

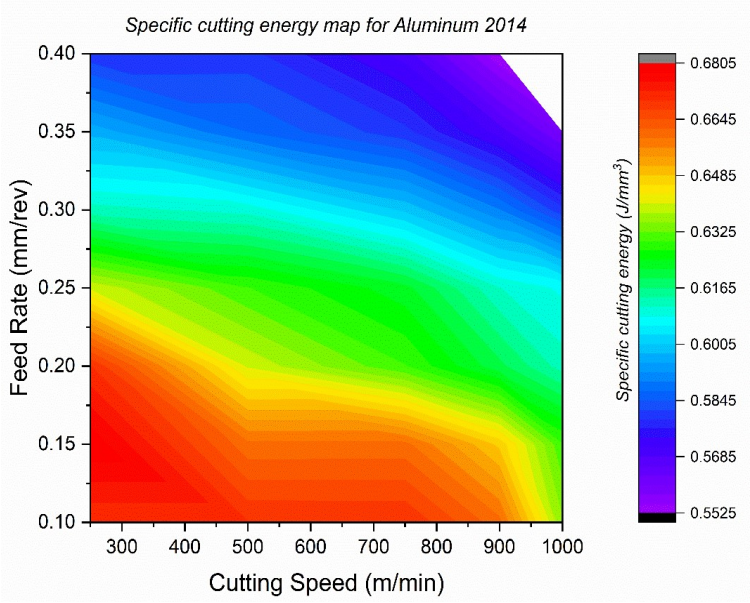

Figure 3. SCE map for the aluminum alloy 2014 bar using uncoated H-13A insert: cutting speed range is between 250 m/min and 1000 m/min and feed rate range is between 0.1 mm/rev and 0.4 mm/rev.

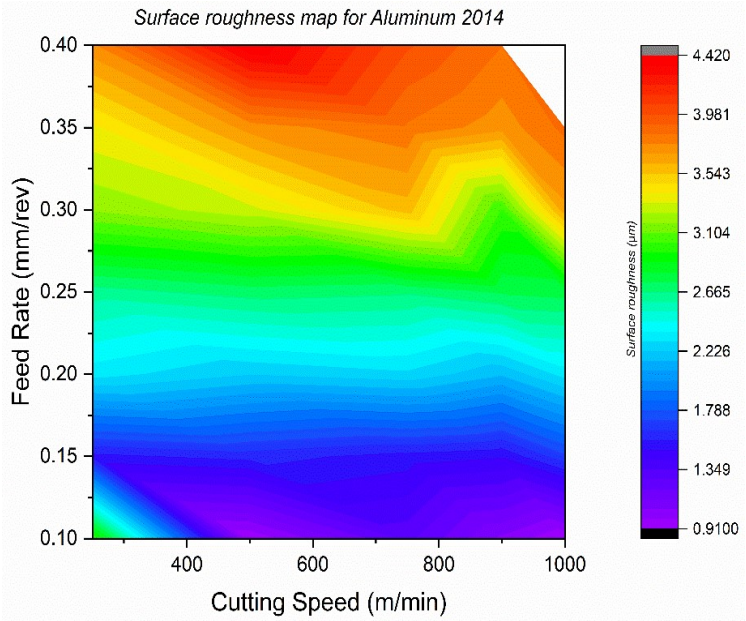

Figure 4. Roughness map for the aluminum alloy 2014 bar using uncoated H-13A insert: cutting speed range is between 250 m/min and 1000 m/min and feed rate range is between 0.1 mm/rev and 0.4 mm/rev.

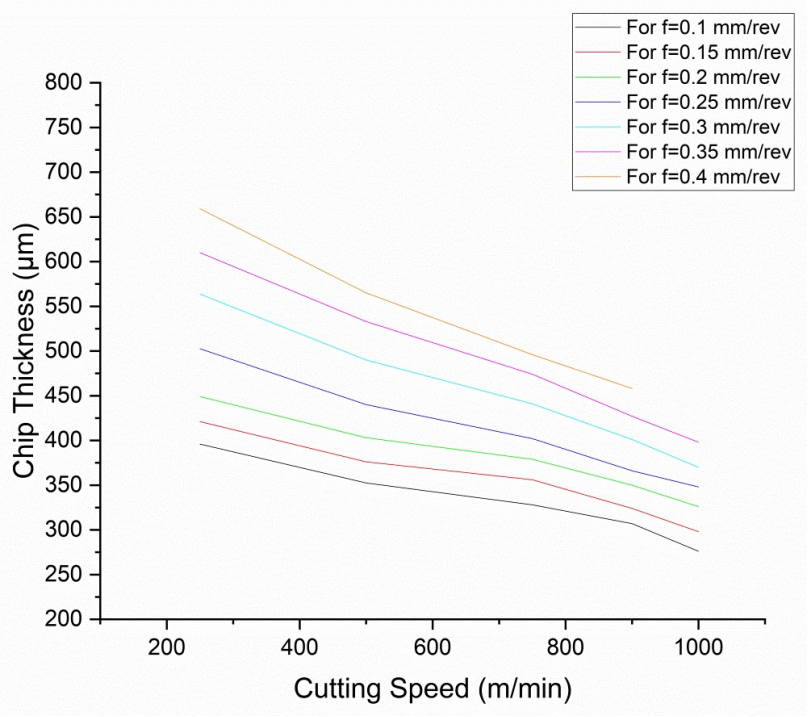

Figure 5. Variation of chip thickness with cutting speed: The changing speed range varies between 250 m/min and 1000 m/mm for the aluminum alloy 2014.

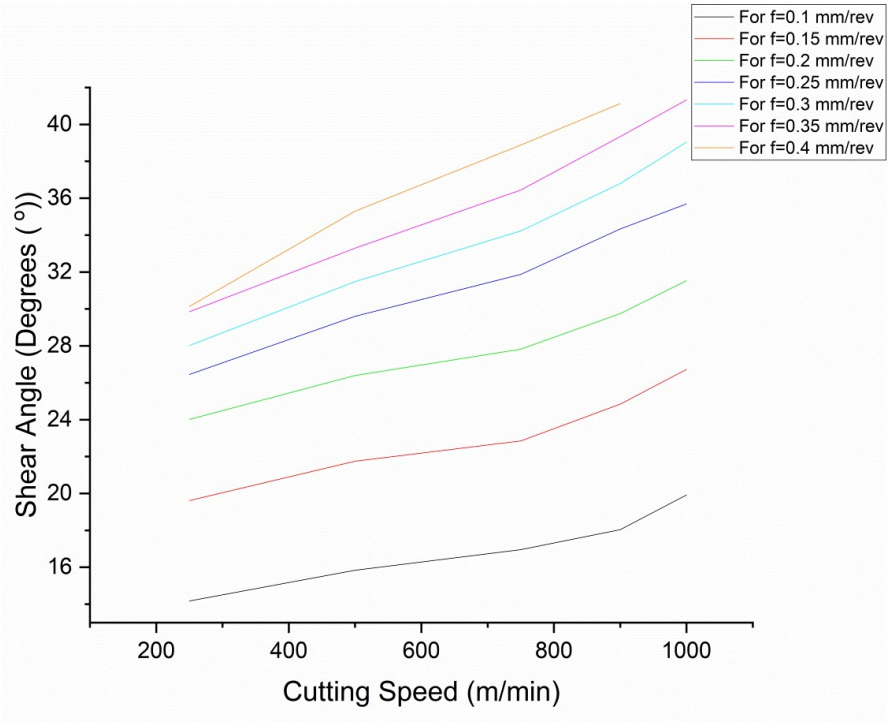

Figure 6. Variation of shear angle with cutting speed: the changing speed range varies between 250 m/min and 1000 m/min for the aluminum alloy 2014.

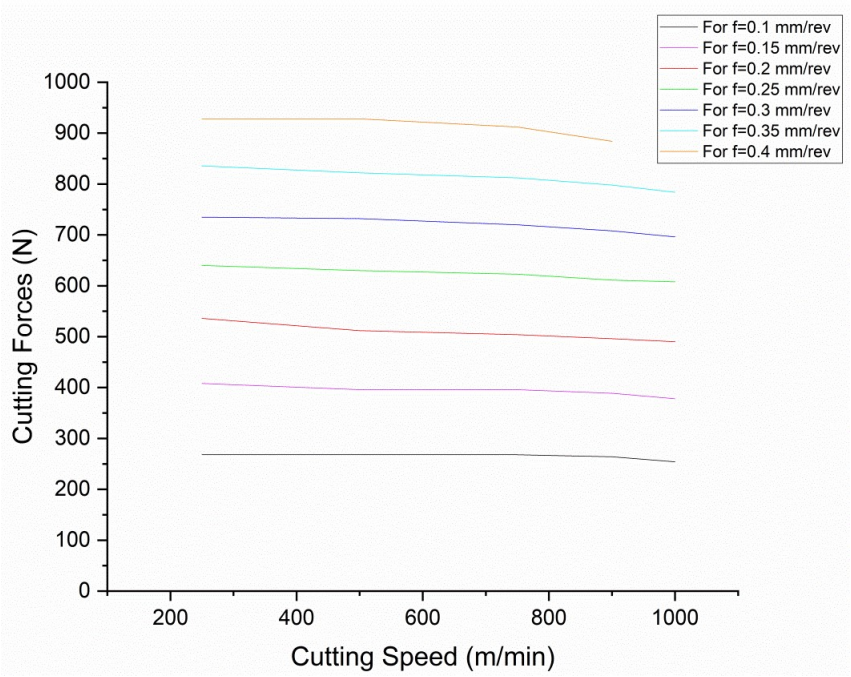

Figure 7. Variation of cutting forces with cutting speed: the changing speed range varies between 250 m/min and 1000 m/min for the aluminum alloy 2014.

The present work is based on the turning of the aluminum alloy 2014 with a selected range of 250 m/min to 1000 m/min for cutting speed. The range for the feed rate was between 0.1 mm/rev to 0.4 mm/rev, with an increment step of just 0.05 mm/rev. The results of the SCE have been complied in order to develop an energy consumption map. Similar work has been performed on the aluminum alloy 6061-T6 by Warsi et al. [24].

Energy consumption for the selected parameters for the aluminum alloy 2014 is depicted in Figure 8. The values of the SCE of respective cutting parameters are presented. It can be observed that with an increase in the feed rate and cutting speed, the specific energy consumption diminishes. Adiabatic heating of the material occurs at moderate cutting speeds, leading to the thermal softening of the material.

Energy consumption for various cutting parameters for the aluminum alloy 6061-T6 has been taken from the literature and are presented in Figure 9. It shows a decrease of energy consumption with an increase in cutting speed. Moreover, energy consumption also faces a decline when the feed rate is increased. Figures 8 and 9 both show a similar trend. The difference appears only in the energy consumption values at the selected machining parameters. A close overview of specific energy consumption illustrates that for the same values of cutting speed and feed rate, the specific energy consumption is higher for the aluminum alloy 2014 as compared to the specific energy consumption for the aluminum alloy 6061-T6. The inclusion of higher percentages of copper in the aluminum alloy 2014 makes it slightly harder than the aluminum alloy 6061-T6. However, the higher hardness of the aluminum alloy 2014 makes it more difficult to cut. Therefore, it experiences higher SCE values when compared to the aluminum alloy 6061-T6.

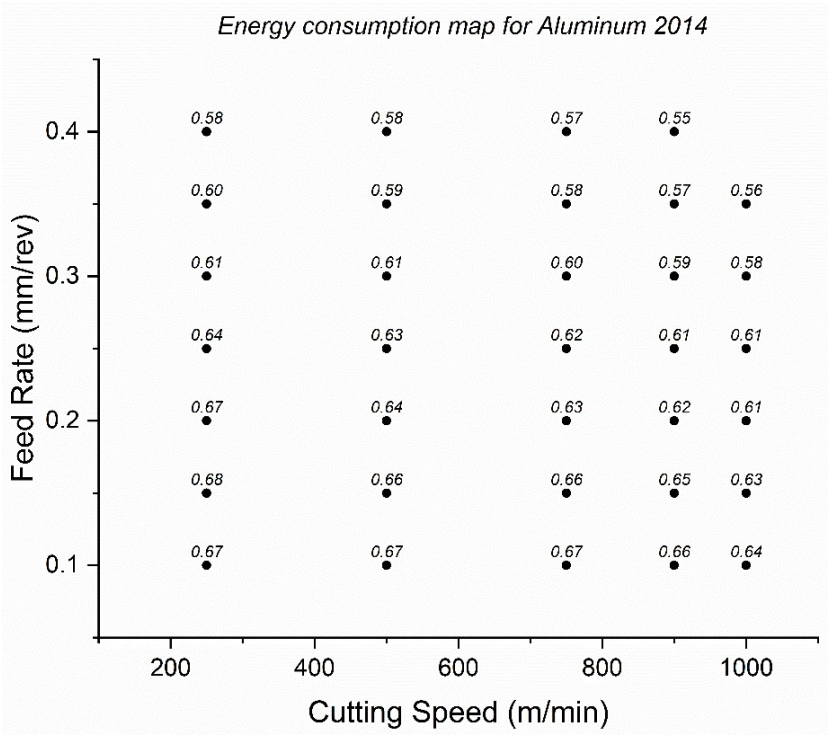

Figure 8. The date associated with energy consumption for the aluminum alloy 2014, which are obtained experimentally in the present study.

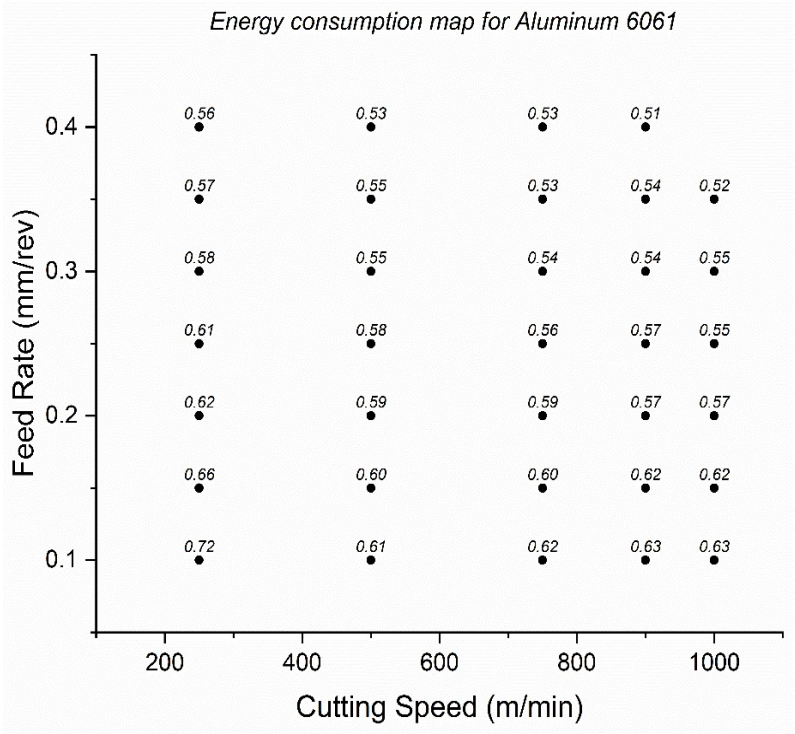

Figure 9. The date associated with energy consumption for the aluminum alloy 6061-T6 in the literature [24].

4. Conclusions

Development and analysis of the SCE and roughness maps for OM was presented in this research. The major findings of this research can be concluded as follows:

- Specific energy consumption decreases at moderate cutting speeds due thermal softening caused by adiabatic heating and a reduced coefficient of friction.
- Increased feed rates result in the increased resistance offered by the material to the machining operation which causes the specific cutting energy and cutting forces to rise.
- Reduced feed rates enhance the surface finish at every cutting speed.
- Chip thickness decreases with increasing cutting speeds, while the shear angle increases with increasing cutting speeds, concluding that the machinability of the material is better at moderate cutting speeds.
- The aluminum alloy 2014 consumes a much higher specific cutting energy when compared to the aluminum alloy 6061-T6 during the machining operation under same machining parameters.

This study is based on both low and medium cutting speeds. This research can be extended to high cutting speeds to extend the SCE and roughness maps to a high cutting speed region. Moreover, the impact of the cutting fluids on the SCE maps can also be studied.

Use of AI tools declaration

The authors declared they didn't use AI, in any form, in the present work.

Acknowledgements

For this work, the funding sources are the mechanical engineering departments of PIEAS and NUST, Islamabad. PIEAS overlooked the availability of the material and NUST overlooked the availability of the inserts.

Conflict of interest

The authors declare that there is not conflict of interest between the authors.

References

1. Morinaga M (2018) *A Quantum Approach to Alloy Design An Exploration of Material Design and Development Based Upon Alloy Design Theory and Atomization Energy Method*, Elsevier.
2. Campbell FC (2006) *Manufacturing Technology for Aerospace Structural Materials*, Elsevier. https://doi.org/10.1016/B978-185617495-4/50011-1
3. Tan Z, Pang B, Oliveira JP, et al. (2022) Effect of S-curve laser power for power distribution control on laser oscillating welding of 5A06 aluminum alloy. *Opt Laser Technol* 149: 107909. https://doi.org/10.1016/j.optlastec.2022.107909
4. Zheng M, Yang J, Xu J, et al. (2023) Interfacial microstructure and strengthening mechanism of dissimilar laser al/steel joint via a porous high entropy alloy coating. *J Mater Res Technol* 23: 3997–4011. https://doi.org/10.1016/j.jmrt.2023.02.040

5. Torenbeek E (2013) *Advanced Aircraft Design: Conceptual Design, Analysis and Optimization of Subsonic Civil Airplanes*, John Wiley and Sons, Ltd. https://doi.org/10.1002/9781118568101
6. Yoon HS, Kim ES, Kim MS, et al. (2015) Towards greener machine tools-A review on energy saving strategies and technologies. *Renew Sustain Energy Rev* 48: 870–891. https://doi.org/10.1016/j.rser.2015.03.100
7. Mead I (2017) International Energy Outlook 2017. Available from: https://www.eia.gov/pressroom/presentations/mead_91417.pdf
8. Zhao G, Hou C, Qiao J, et al. (2016) Energy consumption characteristics evaluation method in turning. *Adv Mech Eng* 8: 168781401668073. https://doi.org/10.1177/1687814016680737
9. Li W, Kara S (2011) An empirical model for predicting energy consumption of manufacturing processes: a case of turning process. *Proc Inst Mech Eng Part B* 225: 643–652. https://doi.org/10.1177/2041297511398541
10. Dahmus JB, Gutowski TG (2004) An environmental analysis of machining. *IMECE04 2004 ASME International Mechanical Engineering Congress and Exposition*, Anaheim, California, USA, 2004: 643–652. https://doi.org/10.1115/IMECE2004-62600
11. Gutowski T, Dahmus J, Thiriez A (2006) Electrical energy requirements for manufacturing processes. *13th CIRP International Conference on Life Cycle Engineering*, Leuven, Belgium, 31: 623–638.
12. Goncharenko AV (2018) Aeronautical and aerospace material and structural damages to failures: Theoretical concepts. *Int J Aerosp Eng* 2018: 1–7. https://doi.org/10.1155/2018/4126085
13. Groover MP (2010) *Fundamentals of Modern Manufacturing: Materials, Processes, and Systems*,Wiley.
14. Li L, Yan J, Xing Z (2013) Energy requirements evaluation of milling machines based on thermal equilibrium and empirical modelling. *J Clean Prod* 52: 113–121. https://doi.org/10.1016/j.jclepro.2013.02.039
15. Benedicto E, Carou D, Rubio EM (2017) Technical, economic and environmental review of the lubrication/cooling systems used in machining processes. *Procedia Eng* 184: 99–116. https://doi.org/10.1016/j.proeng.2017.04.075
16. Kopac J, Pusavec F, Krolczyk G (2015) Cryogenic machining, surface integrity and machining performance. *Arch Mater Sci Eng* 71: 83–93.
17. Krolczyk GM, Maruda RW, Krolczyk JB, et al. (2019) Ecological trends in machining as a key factor in sustainable production—A review. *J Clean Prod* 218: 601–615. https://doi.org/10.1016/j.jclepro.2019.02.017
18. Saleem W, Zain-ul-abdein M, Ijaz H, et al. (2017) Computational analysis and artificial neural network optimization of dry turning parameters-AA2024-T351. *Appl Sci* 7: 642. https://doi.org/10.3390/app7060642
19. Do TV, Hsu QC (2016) Optimization of minimum quantity lubricant conditions and cutting parameters in hard milling of AISI H13 steel. *Appl Sci* 6: 83. https://doi.org/10.3390/app6030083
20. Dhokia V, Newman ST, Imani-Asrai R (2012) An initial study of the effect of using liquid nitrogen coolant on the surface roughness of inconel 718 nickel-based alloy in CNC milling. *Procedia CIRP* 3: 121–125. https://doi.org/10.1016/j.procir.2012.07.022

21. Syed AK, Zhang X, Moffatt JE, et al. (2017) Effect of temperature and thermal cycling on fatigue crack growth in aluminium reinforced with GLARE bonded crack retarders. *Int J Fatigue* 98: 53–61. https://doi.org/10.1016/j.ijfatigue.2017.01.018
22. Caruso S, Rotella G, Del Prete A, et al. (2019) Finite element modeling of microstructural changes in hard machining of SAE 8620. *Appl Sci* 10: 121. https://doi.org/10.3390/app10010121
23. Meng X, Lin Z, Wang F (2013) Investigation on corrosion fatigue crack growth rate in 7075 aluminum alloy. *Mater Des* 51: 683–687. https://doi.org/10.1016/j.matdes.2013.04.097
24. Warsi SS, Jaffery SHI, Ahmad R, et al. (2018) Development of energy consumption map for orthogonal machining of Al 6061-T6 alloy. *P I Mech Eng B-J Eng* 232: 2510–2522. https://doi.org/10.1177/0954405417703424
25. Draganescu F, Gheorghe M, Doicin CV (2003) Models of machine tool efficiency and specific consumed energy. *J Mater Process Technol* 141: 9–15. https://doi.org/10.1016/S0924-0136(02)00930-5
26. Pawade RS, Sonawane HA, Joshi SS (2009) An analytical model to predict specific shear energy in high-speed turning of Inconel 718. *Int J Mach Tools Manuf* 49: 979–990. https://doi.org/10.1016/j.ijmachtools.2009.06.007
27. Balogun VA, Mativenga PT (2014) Impact of un-deformed chip thickness on specific energy in mechanical machining processes. *J Clean Prod* 69: 260–268. https://doi.org/10.1016/j.jclepro.2014.01.036
28. Warsi SS, Agha MH, Ahmad R, et al. (2019) Sustainable turning using multi-objective optimization: a study of Al 6061 T6 at high cutting speeds. *Int J Adv Manuf Technol* 100: 843–855. https://doi.org/10.1007/s00170-018-2759-2
29. Ghosh CS, Rao PV (2018) Specific cutting energy modeling for turning nickel-based Nimonic 90 alloy under MQL condition. *Int J Mech Sci* 146–147: 25–38. https://doi.org/10.1016/j.ijmecsci.2018.07.033
30. Yao Y, Zhu H, Huang C, et al. (2019) On the relations between the specific cutting energy and surface generation in micro-milling of maraging steel. *Int J Adv Manuf Technol* 104: 585–598. https://doi.org/10.1007/s00170-019-03911-y
31. Liu ZJ, Sun DP, Lin CX, et al. (2016) Multi-objective optimization of the operating conditions in a cutting process based on low carbon emission costs. *J Clean Prod* 124: 266–275. https://doi.org/10.1016/j.jclepro.2016.02.087
32. Bhattacharya A, Das S, Majumder P, et al. (2009) Estimating the effect of cutting parameters on surface finish and power consumption during high speed machining of AISI 1045 steel using Taguchi design and ANOVA. *Prod Eng* 3: 31–40. https://doi.org/10.1007/s11740-008-0132-2
33. Bhushan RK (2013) Optimization of cutting parameters for minimizing power consumption and maximizing tool life during machining of Al alloy SiC particle composites. *J Clean Prod* 39: 242–254. https://doi.org/10.1016/j.jclepro.2012.08.008
34. Kosaraju S, Chandraker S(2015) Taguchi analysis on cutting force and surface roughness in turning MDN350 steel. *Mater Today Proc* 2: 3388–3393. https://doi.org/10.1016/j.matpr.2015.07.313
35. Warsi SS, Jaffery SHI, Ahmad R, et al. (2018) Development and analysis of energy consumption map for high-speed machining of Al 6061-T6 alloy. *Int J Adv Manuf Technol* 96: 91–102. https://doi.org/10.1007/s00170-018-1588-7

36. Find your way to gain an edge in steel turning, Sandvik Coromant. Available from: https://www.sandvik.coromant.com/en-us/campaigns/gain-an-edge-in-steel-turning.
37. Iqbal SA, Mativenga PT, Sheikh MA (2009) A comparative study of the tool-chip contact length in turning of two engineering alloys for a wide range of cutting speeds. *Int J Adv Manuf Technol* 42: 30–40. https://doi.org/10.1007/s00170-008-1582-6
38. Shaw MC (2005) *Metal Cutting Principles*, 2nd Eds., Oxford University Press. https://www.scribd.com/document/344789895/Shaw-Milton-C-Metal-Cutting-Principles#
39. Trent EM (1988) Metal cutting and the tribology of seizure: I seizure in metal cutting. *Wear* 128: 29–45. https://doi.org/10.1016/0043-1648(88)90251-7
40. Childs T, Maekawa K, Obikawa T, et al. (2000) *Metal Machining*, Elsevier.
41. Abukhshim NA, Mativenga PT, Sheikh MA (2006) Heat generation and temperature prediction in metal cutting: A review and implications for high speed machining. *Int J Mach Tools Manuf* 46: 782–800. https://doi.org/10.1016/j.ijmachtools.2005.07.024
42. Schmid SR, Kalpakjian S (2015) *Manufacturing Processes for Engineering Materials*, 5th Eds., Pearson Education India.
43. Giridhar D, Vijayaraghavan L, Krishnamurthy R (2010) Micro-grooving studies on alumina ceramic material. *Mater Manuf Process* 25: 1148–1159. https://doi.org/10.1080/10426914.2010.502952
44. Atkins AG (2003) Modelling metal cutting using modern ductile fracture mechanics: quantitative explanations for some longstanding problems. *Int J Mech Sci* 45: 373–396. https://doi.org/10.1016/S0020-7403(03)00040-7
45. Akram S, Jaffery SHI, Khan M, et al. (2018) Numerical and experimental investigation of Johnson-Cook material models for aluminum (Al 6061-T6) alloy using orthogonal machining approach. *Adv Mech Eng* 10: 168781401879779. https://doi.org/10.1177/1687814018797794

Appendix A

The units balances specified for the specific cutting energy (*SCE*) and cutting force (F_c), along with their interpretations, are as follows:

$$\mathrm{SCE}=\frac{\left(\mathrm{P_{cut}}-\mathrm{P_{air}}\right)}{\mathrm{v}\times\mathrm{f}\times\mathrm{d}}=\frac{\mathrm{W}}{\left(\frac{\mathrm{m}}{\mathrm{min}}\right)\times\mathrm{mm}\times\mathrm{mm}}=\frac{\left(\frac{\mathrm{J}}{\mathrm{sec}}\right)}{\left(\frac{\mathrm{m}}{60\,\mathrm{sec}}\right)\times\mathrm{mm}\times\mathrm{mm}}=\frac{\left(\frac{\mathrm{J}}{\mathrm{sec}}\right)}{\left(\frac{1000\mathrm{mm}}{60\,\mathrm{sec}}\right)\times\mathrm{mm}\times\mathrm{mm}}=0.06\left(\frac{\mathrm{J}}{\mathrm{mm}^3}\right)$$

$$\mathrm{F_c}=\mathrm{SCE}\times\mathrm{w}\times\mathrm{t_o}=\left(\frac{\mathrm{J}}{\mathrm{mm}^3}\right)\times\mathrm{mm}\times\mathrm{mm}=\left(\frac{\mathrm{N}\times\mathrm{m}}{\mathrm{mm}^3}\right)\times\mathrm{mm}\times\mathrm{mm}=\left(\frac{1}{0.001}\right)\frac{\mathrm{N}\times\mathrm{m}}{\mathrm{m}}=1000\left(\mathrm{N}\right)$$